Ices of CO_2/H_2O Mixtures. Reflection−Absorption IR Spectroscopy and Theoretical Calculations

Belén Maté,*,† Oscar Gálvez,† Beatriz Martín-Llorente,† Miguel A. Moreno,† Víctor J. Herrero,† Rafael Escribano,† and Emilio Artacho‡

Instituto de Estructura de la Materia, CSIC, Serrano 123, 28006 Madrid, Spain, and Department of Earth Sciences, University of Cambridge, Downing Street, Cambridge CB2 3EQ, United Kingdom

Received: August 31, 2007; In Final Form: October 22, 2007

Ice mixtures of CO_2 and H_2O are studied using Fourier transform reflection−absorption infrared (RAIR) spectroscopy. Mixtures are prepared by sequential deposition or co-deposition of the two components from the gas phase onto an Al plate kept at 87 K inside a low-pressure chamber. Two CO_2 structures are found in most experiments: a crystalline form similar to pure CO_2, which evaporates when warming at 105 K, and a noncrystalline species which remains embedded in amorphous water ice after warming. Significant spectral variations are found depending on the deposition method and the thickness of the solid. Features characteristic of the RAIR technique appear in the spectral regions of the normal modes of the bending and asymmetric stretching CO_2 vibrations. Simulations using Fresnel theory and Mie scattering are carried out with acceptable agreement with the experimental spectra of solids of variable thickness, from ∼1 μm to the limit of nanoparticles. Theoretical calculations of a pure CO_2 crystal are performed. The relaxed geometry of the solid and its vibrational spectrum are determined and compared to the experimental results.

Introduction

The interest in mixed ices of CO_2 and water as laboratory analogues for astrophysical objects has been manifested frequently.[1−3] Mixtures of water and carbon dioxide plus several other compounds such as carbon monoxide, methanol, ammonia, methane, and more, in different concentrations, are known to be present in the frozen nuclei of comets.[4,5] In our solar system, frozen CO_2 is found in various satellites, often with the presence of water.[6−8] Small aggregates forming dust interstellar particles may also contain ices of water and other components, carbon dioxide included.[9−11] In the laboratory, the system CO_2/water ice has been investigated several times, mainly by infrared spectroscopy and mass spectrometry, in temperature programmed desorption (TPD) experiments.[3,12−15] In a recent publication Gálvez et al.[14] have recorded IR transmission spectra of ices of CO_2 and water prepared by sequential deposition or co-deposition of these compounds, detecting through spectral changes two different ways of association between them, either of which may be dominant depending on the temperature and deposition scheme. These spectral variations have been observed before[1,13] in investigations carried out under different conditions.

The technique of reflection−absorption infrared (RAIR) spectroscopy provides information in addition to that obtained in the transmission setup. The possibility of using polarized incident radiation, either in a plane perpendicular to the plane of incidence (S polarization, from the German word *senkrecht*, perpendicular) or in the plane of incidence (P or parallel polarization), allows the observation of molecular vibrations that might be inactive in transmission experiments, for instance, the longitudinal modes in slab-shaped samples when illuminated by normal incidence radiation, which is a standard transmission setup. Besides, the separation of longitudinal and transverse optical modes (the so-called LO/TO splitting)[16] in P-polarized spectra, and the aspect of the spectral region between them, may provide information on the macroscopic shape of the sample.[17,18] These features have encouraged us to undertake the present study, in which ice mixtures of CO_2 and water are prepared by different methods and their spectra are recorded at the deposition temperature, and also after warming at several other temperatures. The results are interpreted in conjunction with those of ref 14.

A close simulation of the experimental systems mentioned above is not possible with our present computing techniques. As a first step in this direction, we have carried out a density functional calculation of the structure of a crystal of CO_2 and a prediction of the corresponding infrared spectrum. We have used the SIESTA method,[19,20] which has provided very reliable results for periodic systems of different types. Although the intermolecular forces for the CO_2 crystal are of the van der Waals type, which is especially complicated to deal with for this kind of calculations, our results seem to display a reasonably accurate picture of the experimental observations.

Theory

Theoretical Calculations of Pure CO_2 Ice. The crystal of CO_2 belongs to the *Pa*3 space group, with a unit cell length $a = 5.624$ Å and a C−O bond distance of 1.155 Å.[21] The C atoms are situated at points of S_6 symmetry, with four CO_2 molecules within the unit cell,[16] linked among them by weak van der Waals forces. This system is particularly ill-suited for study using quantum mechanical methods, and this has forced us to employ high-quality basis functions and fairly strict convergence parameters.

We have performed density functional theory (DFT) calculations with the SIESTA method, under the Perdew−Burke−

* Corresponding author. Fax: (34) 91564 5557. E-mail: bmate@iem.cfmac.csic.es.

† CSIC.

‡ University of Cambridge.

10.1021/jp0769983 CCC: $40.75
Published on Web 01/03/2008

Ernzerhof[22] parametrization of the generalized gradient approximation (GGA), which is more suitable to describe weak intermolecular interactions.[23] The core electrons were substituted by norm-conserving pseudopotentials of the Troullier-Martins flavor, and the basis set for the valence electrons was a linear combination of atomic orbitals (LCAO) at the double-ζ polarized (DZP) level, localized within a soft confining potential[24] whose parameters (kindly provided by M. V. Fernández Serra) were variationally obtained. The employment of a cutoff of 300 Ry for the real space grid and of 6 Å for the *k*-point sampling allows us to achieve an energy convergence better than 10^{-4} eV per atom. The force tolerance parameter has been set to 10^{-4} eV/Å and the stress tolerance to 0.01 GPa.

The prediction of absorption intensities involves the calculation of the Born effective charges, proportional to the variation of the macroscopic polarization of the crystal with atomic displacements.[25] They have been evaluated by numerical derivation of the macroscopic polarization, employing a step of 0.04 bohr, the same that we employed for the force constants calculation. The electronic contribution to the polarization is calculated using the Berry phase formalism,[26] by a discrete integration over the points of a grid, which we fixed in the present case as $5 \times 2 \times 2$, a value that induced a well-converged spectrum. Born charges need only be calculated for the atoms in the irreducible unit of the crystal, from which the appropriate values for the rest of atoms in the unit cell can be deduced by symmetry considerations.

LO/TO Splitting. The separation between the longitudinal and transverse components of optical vibrations in microcrystalline solids has been known and understood for a long time.[16,27,28] More recently, Ovchinnikov and Wight[17,18] have also dealt with this subject in relation to line shapes and broadening effects in IR and Raman spectra of thin films and clusters. Signorell and several co-workers[29−33] have applied the so-called exciton approach to study this effect in CO_2 and other nanoparticles, by means of theoretical calculations, and Bauerecker[34] and Taraschewski et al.[35] have carried out exciting experiments on CO_2 and CO_2/water nanoparticles, where the influence of composition and shape of the particles on their IR spectra is also studied.

Long-range dipole−dipole interactions between molecular vibrations in microcrystalline solids are responsible for absorptions in the spectral range between the transverse optical (ν_{TO}) and longitudinal optical (ν_{LO}) frequencies of a bulk crystal. The appearance of the spectral features in this region can be related to the shape and size of the microcrystals in the sample, assuming that the dimensions of the sample are small compared to the wavelength of the radiation. Spectral band shapes can be calculated analytically for ellipsoidal crystals, or they can be numerically deduced for clusters of particles reaching a fairly large size.[32] In many infrared investigations of molecular crystals, the samples are built as slabs on top of a plate or mirror, and if the incident light is oriented perpendicularly to the slab, only the transverse components of molecular vibrations can be detected at ν_{TO} for single crystals or homogeneous crystallites of oblate type. The same components can be measured in S-polarized RAIR experiments. If, on the other hand, there is a non-null component of the incident radiation along the surface normal, absorptions at the longitudinal frequency, or between ν_{LO} and ν_{TO}, can be measured. This can be achieved if the incident light is tilted with respect to the perpendicular direction to the slab, in transmission or in P-polarized reflection−absorption setups. The appearance of the spectra may not be identical for both techniques; however, as in RAIR experiments reflections play an important role.

In anisotropic samples broadening between ν_{LO} and ν_{TO} is expected for any geometry. Two particularly striking examples are provided by the spectra of samples of 1:1 ratio of ^{12}C and ^{13}C isotopes (see Figure 1(c) of ref 31), and by the spectra of pure CO_2 and N_2O samples obtained by crystallization of CO_2 on an Ar matrix followed by vaporization of the Ar.[18] In general, for samples of different shapes and structures, the form of the corresponding spectrum can be quite different. Some of the possible geometries and expected vibrational bands have been summarized in Table 1 of ref 35.

The splitting between the LO and TO components is related to the strength of the transition by the equation[17]

$$\omega_{LO}^2 - \omega_{TO}^2 = \frac{4\pi}{\epsilon V}\left(\frac{d\mu}{dQ}\right)^2 \quad (1)$$

where V is the unit cell volume, ϵ is the dielectric constant of the crystal, and $d\mu/dQ$ represents the derivative of the transition dipole moment with respect to the Q normal mode. Ovchinnikov and Wight[17] have shown that for isolated vibrational modes the magnitude of the LO/TO splitting depends on the strength of the transition, but the frequency distribution between the two limiting absorption frequencies does not. This is nicely depicted in Figure 1 of ref 17 for all three fundamental molecular vibrations of a N_2O microcrystalline film.

The available optical constants for water and CO_2 crystals[36,37] allow the prediction of spectra of slabs or films of variable thickness both for pure ices and for mixtures, using the well-known Fresnel theory.[38,39] Such calculations were performed by Maté et al.[38] to aid in the interpretation of RAIR spectra of pure water ice. We apply the same technique here to the analysis of spectra of experimental samples of pure CO_2 and of CO_2/H_2O mixtures made by sequential deposition.

Experimental Section

Water/carbon dioxide ices were grown and studied by RAIR spectroscopy using the experimental setup available in our laboratory. A detailed description of the sample preparation is given in ref 14. For the sake of internal consistency of this paper, we present here a short summary of the experimental arrangement and deposition techniques.

The RAIR experiments were conducted in an ultrahigh vacuum (UHV) cylindrical chamber, evacuated by a turbomolecular pump and provided with a liquid nitrogen Dewar flask in contact with the deposition substrate.[40,41] After the Dewar flask was filled, the base pressure was in the 10^{-9} mbar range. Ice was condensed on a substrate made of polished aluminum, whose temperature could be regulated between 87 and 300 K with an accuracy of 1 K. In previous experiments,[38] a gold-coated substrate was also used, and no significant influence was detected on the observed spectra. The infrared beam from a Bruker Vertex 70 Fourier transform infrared (FTIR) spectrometer was directed onto the Al surface at 75° from the surface normal, and the specularly reflected light was collected by a parabolic mirror onto a liquid nitrogen cooled mercury cadmium telluride detector. A polarizer (SPECAC KRS-5) was used to select the polarization of the incident radiation. Each spectrum was obtained by addition of between 256 and 512 scans recorded at 2 cm^{-1} apodized resolution. Two independent inlets, for water and carbon dioxide, were used to introduce the vapors and to backfill the chamber. The purity of the species introduced into the chamber was measured with a quadrupole mass spectrometer. The ice film thickness could be approximately measured

(with an estimated uncertainty of ±10%) by monitoring the interference fringes of a He−Ne laser incident on the growing film at near-normal incidence.

Samples of mixed water/CO_2 ices were prepared by the following four types of deposition methods:

Crystalline Sequential (CS) Deposition: Water is first deposited at 87 K. The temperature is then raised to 165 K and kept there for 5 min in order to induce crystallization from the amorphous phase. The crystalline water film is subsequently cooled to 87 K, and then CO_2 is admitted until the desired H_2O/CO_2 ratio is achieved.

Amorphous Sequential (AS) Deposition: Water is first deposited at 87 K as amorphous solid (ASW), and then CO_2 is added at the same temperature, until the chosen ratio is accomplished.

Co-deposition (CD): Water and CO_2 are introduced into the chamber simultaneously, at the appropriate ratio, and deposited on the substrate at 87 K.

Inverse Sequential (IS) Deposition: First the desired amount of CO_2 is introduced into the chamber with the substrate at 87 K. At this temperature, crystalline CO_2 is expected to form. Then water is admitted, keeping the substrate always at 87 K, until the chosen water/CO_2 ratio is reached.

The ice mixtures were prepared for different water to carbon dioxide ratios, with partial pressures in the $10^{-6}-10^{-5}$ mbar range. CO_2 dosing in all experiments but co-deposition corresponded always to a thickness growing at approximately 1.5 nm/s. For water, the deposition rate varied between 10 nm/s in CS, 6 nm/s in AS, and 4 nm/s in IS experiments. In co-deposition experiments the H_2O/CO_2 proportion was obtained by adjusting both the H_2O and CO_2 pressures, with the result of a deposition rate variation from 6 nm/s for 3:2 and 7:2 mixtures to 14 nm/s in 7:1 mixtures. The deposition rate may alter the physical properties of the ices formed, as discussed in previous literature.[12] The first spectra were always recorded at the lowest temperature, ~87 K. The samples were subsequently warmed to 105 K, and then new spectra were taken. The largest spectral variations were observed at this temperature. More spectra were recorded after warming at 140 and 165 K. The spectra did not show any appreciable changes between 105 and 140 K, but at the highest experimental temperature, 165 K, practically all the CO_2 had been removed from the samples. For the crystalline sequential case, all CO_2 was already evaporated at 105 K.

Results and Discussion

Calculations of Pure CO_2 Crystals. With the methodology and parameters described above, the lattice parameter was calculated by fitting the cohesion curve to a cubic spline, and the internal structure was relaxed within the theoretical cell. The relaxed structure complies in a satisfactory manner with the experimental symmetry, with a slight overestimation of the unit cell length and also of the C−O bond distance (calculated values $a_{calc} = 5.701$ and 1.184 Å, respectively).

Previous theoretical calculations on the structure of this and other high-pressure phases of CO_2 had been performed using both semiempirical[42,43] and ab initio methods.[23,44,45] The calculations by Gygi,[23] with the same exchange correlation functional as in this work but with plane waves instead of atomic orbitals as the basis set, yielded a slightly closer approximation to the experimental lattice parameter. These calculations reveal the importance of the more rigorous treatment of the quadrupole−quadrupole intermolecular interactions as the reason for their good agreement with experiment. Dows and Schettino[46] have evaluated the dispersion curves of phonons in solid CO_2 by means of a theory of two-phonon states appropriate to vibrational excitations in molecular crystals. Our calculations of dispersion curves give a reasonable match to those of Figure 6 of Dows and Schettino.[46]

TABLE 1: Calculated Wavenumbers (in cm^{-1}) and Intensities (in Atomic Units: charge^2 mass^{-1}) for the Normal Modes of Crystalline $^{12}CO_2$ and $^{13}CO_2$ after Relaxation with SIESTA[a]

normal mode	$^{12}CO_2$	$^{13}CO_2$	int
ν_2	601.4	584.6	0.07
	601.4	584.6	0.07
	601.4 (2.6)	584.6 (2.6)	0.07
	602.0	585.2	0
	602.0	585.2	0
	606.7	589.8	0.12
	606.7	589.8	0.11
	606.8 (16.2)	589.8 (15.6)	0.11
ν_1	1295.0	1295.0	0
	1295.0	1295.0	0
	1295.0	1295.0	0
	1295.1	1295.1	0
ν_3	2291.2	2226.4	0
	2302.5	2237.7	1.04
	2302.5	2237.7	1.04
	2302.6 (29.5)	2237.7 (28.8)	1.04

[a] The LO/TO splitting is indicated in parentheses for the appropriate ν_{TO} mode.

Using the Born charges calculated as mentioned above, the infrared spectrum can be predicted for the relaxed geometrical structure. The calculated frequencies and absorption intensities for the optical modes of $^{12}CO_2$ and $^{13}CO_2$ crystals are summarized in Table 1. A few remarks are worth noting regarding this table. When going from the free molecule symmetry, $D_{\infty h}$, to the unit cell symmetry, T_h,[16] the internal modes split into the following symmetry species: the Σ stretching modes, Σ_g^+ for ν_1 and Σ_u^- for ν_3, become A and F, keeping their parity g or u; the degenerate Π_u bending mode (ν_2) becomes E_u and F_u; of these only the F_u modes are infrared active. Intermolecular interactions in the crystal cause the two F_u components of ν_2 to split and appear as a doublet in the IR spectrum, labeled as ν_{2a} and ν_{2b}. This well-known spectral structure is satisfactorily accomplished in the calculation: the four bands expected in the ν_3 region are split into one at lower frequency and null intensity and three degenerate and intense bands at a slightly higher frequency. Similarly, each component of the ν_2 mode is split into one plus three components with characteristics similar to those of ν_3. All vibrations corresponding to the ν_1 mode are predicted with zero intensity. The calculated values of the frequencies are lower than the experimental ones, about 8% for ν_2 and 2% for ν_3. The C−O bonds seem therefore to be slightly weaker in the computed crystal than in the experimental structure, as a result of the limitations of the present model consistent with slightly larger bond lengths.

The VIBRA utility of the SIESTA method also enables the estimation of the splitting between transverse and longitudinal modes, if the high-frequency dielectric tensor is known. We have used in our case the value at $\lambda = 1.1$ μm, $\epsilon = 1.99$.[47] The calculated LO/TO frequency shifts are indicated in parentheses for the split modes in Table 1. The three components of ternary symmetry of the ν_2 and ν_3 modes in the unperturbed model are split into two transverse modes of unchanged frequency, plus one longitudinal mode blue shifted with respect to the unperturbed calculation. The calculated splitting values (~16 and 30 cm^{-1} for ν_{2b} and ν_3, respectively) are in reasonable agreement with the observed ones (18 and 37 cm^{-1}).[46]

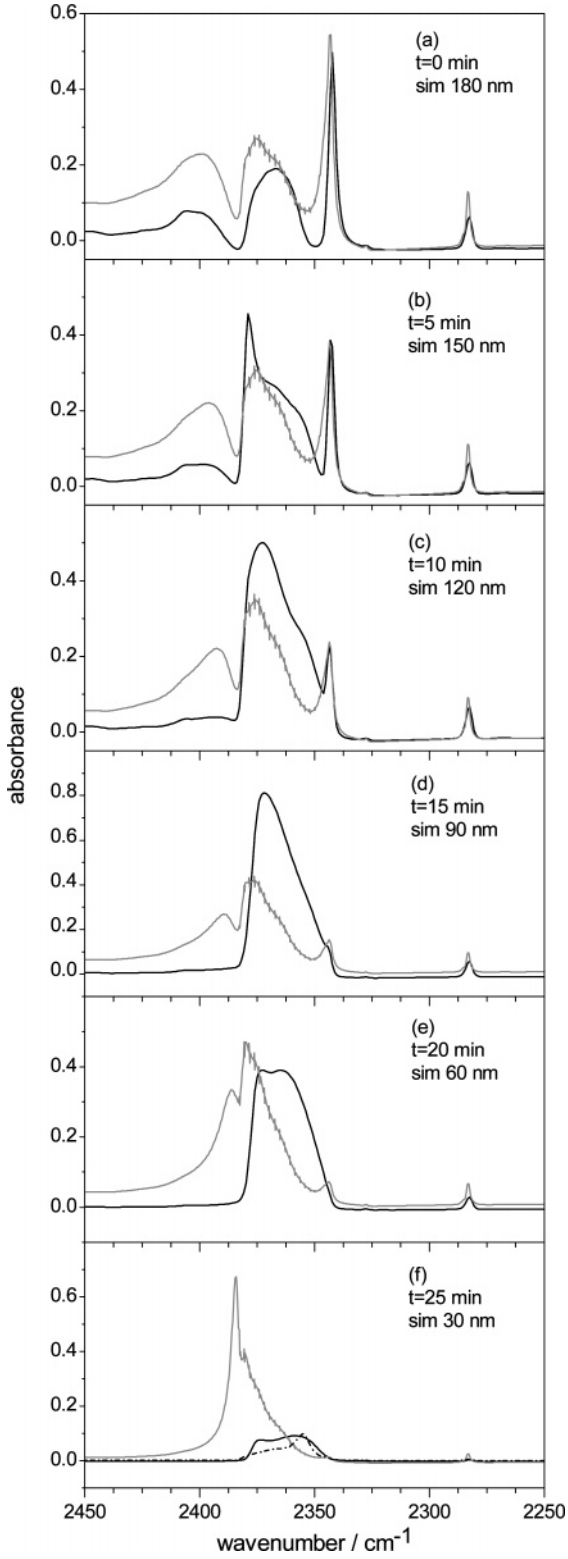

Figure 1. P-polarized RAIR spectra of CO_2 in the ν_3 region recorded at specified time intervals after deposition of CO_2 at 90 K. Solid lines: black, experimental spectra; gray, Fresnel simulations for the indicated thickness. Dashed line (in panel f), Mie scattering spectra of spheres with 10 nm diameter.

Experimental Spectra. *Pure CO_2.* A film of CO_2 of approximately 180 nm was deposited on the Al substrate at 90 K. At this temperature, once the CO_2 flow into the chamber was stopped, the solid began to desorb, and spectra were taken at consecutive 5 min intervals. Figure 1 displays P-polarized RAIR spectra of CO_2 in the ν_3 region at the beginning of the desorption experiment, and at consecutive 5 min intervals. The spectra of CO_2 films can be simulated using the optical indices and the equations of Fresnel.[38,39] Taking the optical constants from ref 36, obtained from normal incidence transmission experiments of vapor deposited CO_2 films at 80 K, we have carried out simulations for the observed spectra by fitting the thickness of the films. The best agreement with the experimental contour is obtained for simulations which decrease linearly in size for the thicker films. When the crystals are thinner, the simulations are no longer satisfactory, and we have chosen the indicated thickness values for the simulations rather arbitrarily. These simulations are included in the figure and discussed in more detail below.

The feature at $\sim$2400 cm^{-1} (Figure 1, panels a−c) is due to an optical effect of the RAIR technique that varies with the thickness of the solid, and does not correspond to molecular vibrations, which are limited to the zone between the LO and TO components, 2381 and 2344 cm^{-1}, respectively.[35,46] This feature is not seen in transmission or in S-polarized experiments, but it is present in the spectra and simulations for thicknesses above 100 nm. On the other hand, the individual LO peak, visible in oblique incidence transmission spectra,[13] is not seen in these RAIR spectra, which consist of a complicated addition of absorption and reflection contributions that hide that particular peak. As a check of the consistency of theory and experiment, we have performed simulations of transmission spectra of CO_2 films with oblique incident light, using the same set of optical constants.[36] The simulations that reproduce reasonably well the shape of our RAIR spectra for films of thickness >100 nm (panels a−c) do also predict the LO peak in transmission spectra of films of similar thickness. With decreasing thickness (panels d−f), the agreement becomes gradually worse and the thin film model of Fresnel cannot account satisfactorily for the observations. For the thinner films a Mie scattering calculation assuming spherical CO_2 particles with a 10 nm diameter[48,49] provides a better reproduction of the observed contour, as depicted in panel f in Figure 1 after appropriate scaling to match the intensity of the experimental trace. The Mie scattering spectrum has been found to be insensitive to the diameter of the particle as long as it is much smaller than the wavelength of the radiation.

The sequence of spectra show that the slab of CO_2 formed when it is admitted to the chamber becomes gradually thinner until the microcrystals of which it is composed are so small and separated that long-range dipole forces are too weak among them.[18] These microcrystals have inhomogeneous shapes, inducing a broad spectral contour. For thicknesses around 90 nm, when the ν_{TO} peak characteristic of slab structures is no longer seen, the spectra resemble more closely those of aerosols or nanoparticles.[33−35] At this point, the Fresnel theory, based on slabs of infinite length, fails to yield a valid reproduction of the experiment, whereas the Mie spectrum gives a closer accord. A similar behavior was observed by Mitlin and Leung[50] for vapor deposited water ice films.

As mentioned above, the relatively good agreement between simulations and experiments for films of CO_2 of thickness larger than 100 nm is a test of the quality of the available optical constants of Ehrenfreund et al.[36] However, a perfect reproduction is not reached because of the difficulty of deriving the real part of the refractive index n in this spectral region from normal incidence transmission experiments, as pointed out by Palumbo and Baratta.[37]

Mixed CO_2/Water Ices. We have carried out a systematic study, changing the CO_2 and H_2O proportions, in all four deposition techniques, to separate optical effects from morpho-

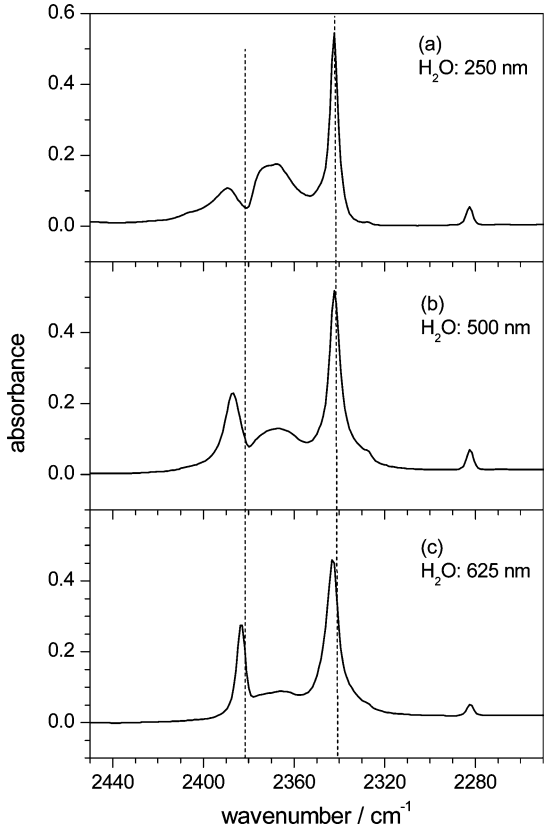

Figure 2. P-polarized RAIR spectra of samples prepared by deposition of CO_2 on crystalline water ice of different thicknesses: 250, 500, and 625 nm, from top to bottom. The thickness of the CO_2 layer is ~100 nm. The position of the theoretical ν_{LO} and ν_{TO} modes is indicated by dashed vertical lines.

logic or internal changes in the samples. We will show our results, discussing the crystalline sequential (CS) and amorphous sequential (AS) depositions first and then co-deposition (CD) and inverse sequential (IS) deposition experiments. We will focus on the changes on the CO_2 bands (asymmetric stretch ν_3, bending ν_2, and combination bands $\nu_1 + \nu_3$ and $2\nu_2 + \nu_3$) in the different experiments, where spectral modifications due to the presence of water are large. Changes in the water bands are not the object of this investigation. They have been dealt with in previous works (see, for instance, the recent paper by Öberg et al.[51] and references therein).

Figure 2 displays P-polarized RAIR spectra in the CO_2 ν_3 region of CS experiments where a fixed amount of CO_2, estimated as a 100 nm layer, was deposited on crystalline water ice of increasing thickness values of 250, 500, and 625 nm, shown top to bottom. Whereas the ν_{TO} peak, at ~2340 cm^{-1} as indicated by a dashed line in the figure, is almost unaffected by the size of the water layer underneath, the aspect of the high-frequency feature and the intermediate region present some interesting variations. The high-frequency peak is caused by interference effects characteristic of the RAIR technique, as commented on above for pure CO_2, and cannot be attributed to the ν_{LO} band, whose frequency is pointed out by a dashed line in the figure. Such interferences shift typically in frequency and width with varying thickness of the layers.[38] Another example of this progression can be followed in the discussion below.

Figure 3 presents P-polarized RAIR spectra of samples prepared by continuous admission of CO_2 on crystalline (left) and amorphous (right) water layers of width ~600 nm. The interference effect responsible for the high-frequency feature around 2380 cm^{-1} displaces this band toward higher frequencies

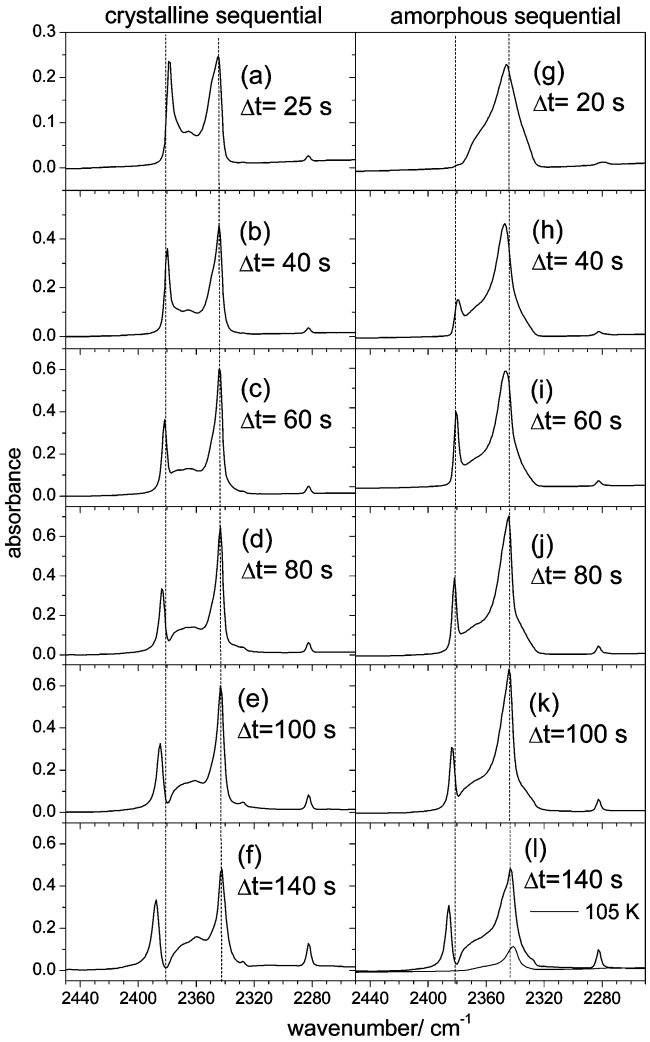

Figure 3. P-polarized RAIR spectra of samples prepared by continuous admission of CO_2 on crystalline (left) and amorphous (right) water layers of width ~600 nm. Spectra were recorded at the indicated times of CO_2 dosing after the water ice was prepared. Samples at the final dosing (140 s) had total thicknesses of ~800 nm (CS) and ~750 nm (AS). On the bottom panel of the AS series, the spectrum after heating at 105 K is included (gray trace).

for larger CO_2 solids for both CS and AS experiments. The spectral features in the CS series, which also constitute the main part of the spectra in AS experiments, are assigned to CO_2 in crystalline domains, with a structure close to that of bulk CO_2 ice, being in contact with the water surface. This structure has been called CO_2-ext,[14] and is vaporized upon heating. The ν_{TO} peak appears always broader in the AS spectra due to a low-frequency shoulder, which stands out as an isolated peak when the sample is heated at 105 K, but which is present in all AS spectra. Spectral features associated with crystalline CO_2 are absent after 20 s deposition, but are already evident after 40 s (see panels g and h). We can assume that saturation of the ASW film takes place some time in between. Taking into account that the ASW layer has a thickness of 600 nm (~1550 monolayers) with a density of ~0.8 g/cm^3,[52] the amount of CO_2 reaching the ice within the 20−40 s time interval corresponds to a CO_2/H_2O molecular ratio in the range $(2.7-5.5) \times 10^{-2}$, as derived from simple gas kinetic theory considerations for a gas temperature of 300 K and a pressure of 10^{-5} mbar. In principle the gas molecules are expected to accumulate in the ice until its entire surface is covered with a CO_2 monolayer. Assuming a mean seat area of 15.5 $Å^2$ per adsorbed CO_2

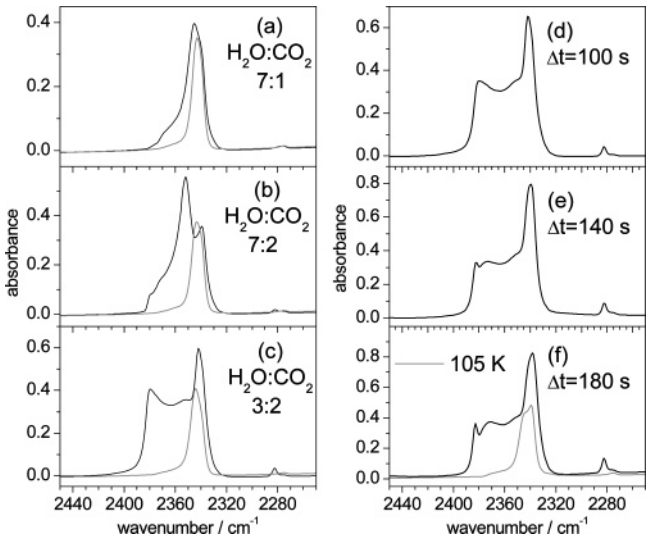

Figure 4. P-polarized RAIR spectra of samples prepared by co-deposition of mixtures of water and CO_2. Left: samples with an approximately equal thicknesses of ~600 nm and water/CO_2 ratios of 7:1, 7:2, and 3:2, top to bottom. Right: a constant mixture of the 3:2 ratio is continuously admitted into the chamber, and spectra are shown at the specified time after the start of the experiment. The corresponding samples had thicknesses of ~600, 840, and 1080 nm, top to bottom. Black, spectra recorded at 87 K; gray, spectra recorded after heating at 105 K.

molecule,[1,53] a specific surface area of 140−280 m^2/g would be needed to accommodate all the CO_2. There is a large disparity in the literature data for the specific surface area of amorphous ice samples, but most values for the 80−90 K interval are in the ~100−400 m^2/g range (see refs 54−57 and references therein) and are thus compatible with the present observations. It is interesting to note that, applying the same considerations to the conditions of the recent experiment of Kumi et al.,[13] similar results (CO_2/H_2O molecular ratios of $(3.2-6.4) \times 10^{-2}$ and specific surface areas of 188−380 m^2/g) are obtained for the saturation of much thinner (≈65 monolayers) ASW films with CO_2.

The low-frequency shoulder on the ν_{TO} peak in AS spectra is attributed to CO_2 embedded in the amorphous water structure, designated as CO_2-int.[14] The lack of high-frequency features accompanying the CO_2-int band, as seen in the 105 K trace of the bottom AS panel (Figure 3, panel l), indicates that the corresponding CO_2 molecules are not occupying any kind of crystalline network or lattice with a repetitive structure, and they will therefore be trapped in internal channels or cavities within the amorphous ice.[13,14,18] When carbon dioxide is deposited on amorphous water ice, it immediately finds its way into the water solid forming CO_2-int. The thickness of the ice, as controlled with a He−Ne laser, showed no apparent growth in the initial stages of CO_2 admission. When more carbon dioxide is added, CO_2-ext is formed, at the water surface, yielding the characteristic spectrum of the solid, with a strong peak at ν_{TO} and spectral features in the higher frequency region, which change with growing thickness of the CO_2 layer, as seen in the sequence of spectra. In spectra of crystalline ice samples, the CO_2-int band is never present, due to the lack of porosity of the corresponding surfaces which prevents CO_2 from entering the ice structure.

Co-deposited Samples. Figure 4 presents P-polarized RAIR spectra of samples prepared by the co-deposition (CD) scheme. On the left we show the spectral variations corresponding to increasing amounts of CO_2 on samples having approximately equal thickness, ~700 nm. The water/CO_2 ratios are 7:1, 7:2, and 3:2, top to bottom. The spectra present a growing intensity in the intervening region between the theoretical ν_{LO} and ν_{TO} wavenumbers, indicating that the amount of irregular microcrystals of CO_2-ext is also increasing relative to that of CO_2-int, which is practically constant in the sequence, as revealed by the corresponding characteristic band which remains after heating at 105 K. The interference effect that we have discussed before also affects the broad structure in the intermediate region, and the typical peak at $\nu > \nu_{LO}$ can be appreciated at ~2385 cm^{-1} in spectrum c.

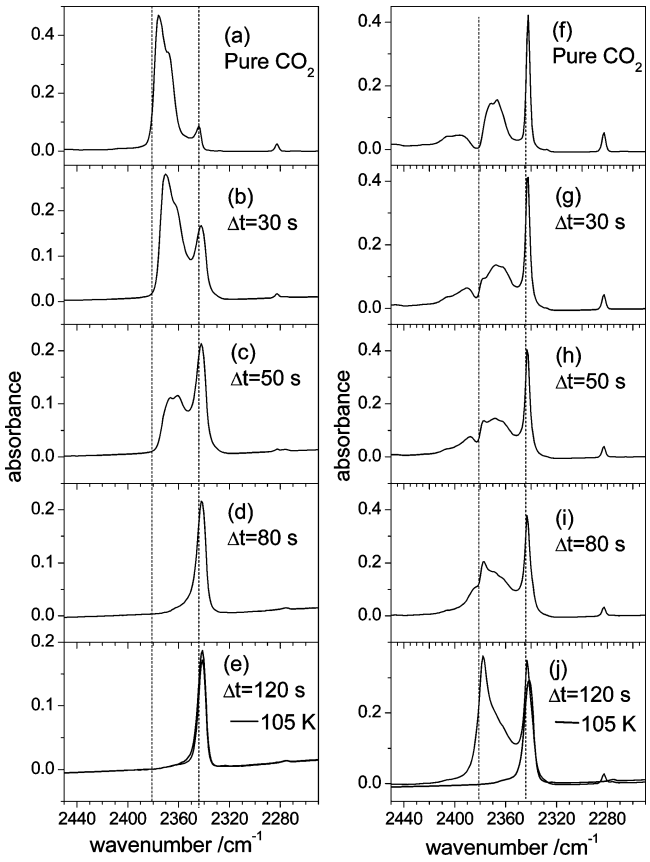

Figure 5. Variations in P-polarized RAIR spectra of samples prepared by inverse sequential deposition. Crystals of pure CO_2 (thicknesses: left, ~100 nm; right, ~180 nm) were prepared (top spectra), and water was then added continuously. Spectra were taken at the indicated times after the start of the experiments. Black, spectra recorded at 87 K; gray, spectra recorded after heating at 105 K.

A complementary experiment gives rise to the spectra represented on the right-hand panels of Figure 4. A mixture of water and CO_2, in the approximate ratio of 3:2, is continuously admitted into the chamber, and spectra are taken at the indicated times after the start of the experiment. Consequently, the spectra correspond to samples growing in thickness from top to bottom. The interference peak characteristic of these RAIR spectra can be seen to tear off toward higher frequencies along the series. The broad structure between ν_{LO} and ν_{TO}, characteristic of inhomogeneous microcrystals, is almost unchanged in this sequence of measurements. The shape of this band depends therefore on the relative concentration of water and CO_2, but not on the thickness of the crystal. The band due to CO_2-int is the only band that remains when the sample is heated and all CO_2-ext is evaporated.

Inverse Sequential Deposition. The last type of deposition method is discussed next. Figure 5 collects P-polarized RAIR spectra of samples prepared in the inverse sequential (IS) deposition scheme. The top spectra are of pure CO_2 crystals.

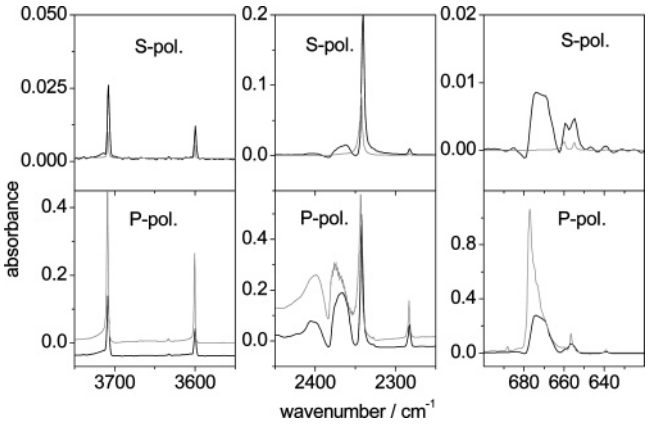

Figure 6. RAIR spectra of pure CO_2 recorded using S-polarized (above) and P-polarized (below) incident IR radiation, in the spectral regions of the combination bands $\nu_1 + \nu_3$ and $2\nu_2 + \nu_3$, the asymmetric stretch ν_3, and the bending mode ν_2, left to right. Solid lines, experimental spectra; gray, Fresnel simulations for a thickness of 180 nm.

The left and right panels correspond to experiments in which the initial thickness of these crystals was ~100 and ~180 nm, respectively. Going down in the figure are shown spectra taken after admitting water into the chamber. The effect of water addition is different in the two series. When the CO_2 crystal is thicker (right), the basic structure of the ν_3 band of pure CO_2 is maintained initially, although an interference peak at $\nu \leq \nu_{LO}$ starts to show after 30 s (panel g) and grows in intensity in the next panels. In the 80 s spectrum (panel i), the ν_{TO} peak typical of CO_2-ext becomes slightly broader than that in previous measurements because of the appearance of the characteristic CO_2-int peak, at slightly lower frequency. The CO_2-int becomes larger at $\Delta t = 120$ s (panel j), and as in previous experiments, it is the only band to remain after the sample is heated at 105 K. When starting with a thinner CO_2 film (left), the CO_2-int peak is already visible after 30 s, and the bands of the CO_2-ext crystalline structure become weaker with further water addition. After 120 s (panel e), all CO_2 is in the form of CO_2-int, and the spectrum does not change when the crystal is heated from 87 to 105 K. Thus, for larger water to carbon dioxide ratio (left panels), the amorphous water layer formed by H_2O addition can take in its interior all CO_2 molecules, which do not adopt any crystalline structure. When the relative amount of carbon dioxide is higher, part is kept forming external layers, and part is accommodated into the ASW. The inclusion of carbon dioxide molecules into the amorphous water structure is probably caused by the mobility of the CO_2 molecules at the temperature of this experiment, which allows them to enter the amorphous water pores or microchannels.

The ν_2 Band and the Combination Bands. The ν_3 band of CO_2 has been more frequently revised in the literature, being the most intense infrared band in a more favorable experimental region, but the symmetric bending mode ν_2, at ~650 cm^{-1}, and overtone and combination bands, near ~3600 cm^{-1}, also provide interesting information.

We present in Figure 6 spectra of a sample of pure CO_2 recorded using S-polarized (above) and P-polarized (below) incident IR radiation, split into the three spectral regions of interest, together with Fresnel simulations for a film 180 nm thick, which is the estimated value of the experimental sample. The central region for the P-polarization is a reproduction of panel a of Figure 1. Note the different intensity values on each vertical panel. Optical effects implicit in the RAIR technique can distort considerably the spectra with respect to transmission

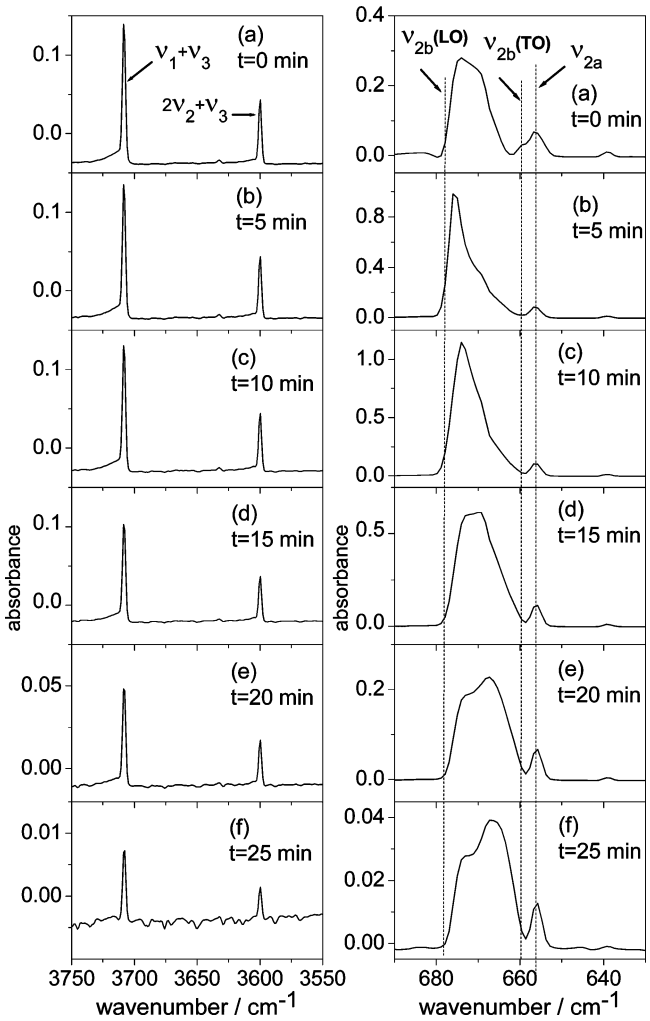

Figure 7. P-polarized RAIR spectra of pure CO_2 in the $\nu_1 + \nu_3$ and $2\nu_2 + \nu_3$ (left) and ν_2 (right) spectral regions, in the same sequence as in Figure 1 above, i.e., taken at 5 min intervals after an initial deposition of CO_2 at 90 K.

experiments and induce the observed intensity differences between the two polarization schemes. Also, the metal surface selection rule (MSSR),[58] which tends to cancel out the signals of some surface vibrations in thin films, affects more substantially the weaker bands in the S-polarized spectra, like the ν_2 mode. Although the simulations do not reproduce correctly the observed intensities, they do follow similar variation trends when the P- and S-polarization experiments are compared.

We display in Figure 7 P-polarized spectra of pure CO_2 in the $\nu_1 + \nu_3$ and $2\nu_2 + \nu_3$ (left) and ν_2 (right) spectral regions, in the same time sequence as in Figure 1 above, i.e., taken at 5 min intervals after an initial deposition of CO_2 at 90 K. The bending vibration is a degenerate mode of Π_u symmetry in the gas phase which gives rise to two nondegenerate, infrared active components of F_u symmetry in the crystal, ν_{2a} and ν_{2b}, at 655 and 660 cm^{-1}, respectively.[59] Only the latter has an appreciable LO/TO splitting (18 cm^{-1}). The position of all three components is indicated by broken vertical lines in the figure. The variation of the ν_{2b} band with time follows the same pattern as for ν_3, with a broad feature between ν_{TO} and ν_{LO} which changes as the solid gets thinner and smaller. It is interesting to see the apparent intensity gain in this region from panels a to c, when some CO_2 has already evaporated, due to an interference effect similar to that encountered before. The ν_{TO} component, which became increasingly weak in the sequence for ν_3, is already very weak in panel a of this figure and cannot be identified in

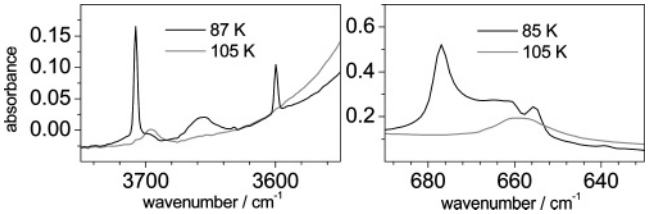

Figure 8. P-polarized RAIR spectra in the regions of the combination bands (left) and of ν_2 (right) of a sample of ~1000 nm thickness prepared by continuous admission of a 3:2 water/CO_2 mixture. Black, spectra recorded at 87 K; gray, spectra recorded after heating at 105 K.

further spectra in the series. Interestingly, since the ν_{2a} component is not split, this band keeps its shape and position unchanged along the series and only loses intensity. The same trend is followed by the combination bands $\nu_1 + \nu_3$ and $2\nu_2 + \nu_3$, measured at 3708 and 3600 cm^{-1}, respectively,[46] depicted in the left-hand-side panels, of which only the intensity changes along. The ν_2 band of the $^{13}CO_2$ isotopomer can be seen at 639 cm^{-1}, stronger in the upper panels. The combination bands of the $^{13}CO_2$ species are too weak to be detected in these spectra.

Finally, Figure 8 presents P-polarized spectra of a CD sample in the regions of ν_2 (right) and of the combination bands (left). The sample is the same as that depicted in panel c of the right-hand side of Figure 4 for the ν_3 band, and the spectra taken after heating the sample at 105 K are also shown as gray lines. The experiment consisted of a continuous admission of a water and CO_2 gas mixture at a fixed 3:2 water to CO_2 ratio. Although not shown here, the trend along the sequence of spectra taken at 40 s intervals is similar to that discussed for ν_3, i.e., an intensity increase of all features as the crystal becomes thicker. The most relevant result concerning the bands described in this section is contained in Figure 8. The ν_2 spectrum of the "cold" sample is similar to that of pure CO_2, with a sharp ν_{2a} peak and a broad feature between the LO and TO components of ν_{2b}, including a strong interference peak near the high-frequency limit. However, the trace of the "warm" sample presents just one single band at the middle frequency between ν_{2a} and ν_{2b}, indicating that the degeneracy of this mode is not removed by crystalline effects for the CO_2-int species. This is again a confirmation of the lack of slab or crystal structure in CO_2-int, embedded in the amorphous water pores.

In the high-frequency region, two features call our attention. A broad band appears at ~3657 cm^{-1} in the spectrum of the sample at 87 K. Bernstein et al.[15] observed a broad structure, centered at ~3648 cm^{-1}, in the spectrum of a $H_2O/CO_2 = 5$ mixture recorded at 15 K, and assigned this band to "dangling" OH bonds. On the other hand, in the spectrum of a thick CO_2 crystal[46] a similar feature can be seen at ~3655 cm^{-1} in the midst of many sharp and broad peaks corresponding to transitions involving two phonons or even higher order effects. Since none of these extra features are seen in our spectrum, we tend to agree with the interpretation of Bernstein et al.[15] The spectrum of CO_2-int, the only carbon dioxide species that remains at 105 K, presents just one peak, at 3695 cm^{-1}, broader and red shifted with respect to $\nu_1 + \nu_3$ of CO_2-ext. The interpretation of this peak is not unambiguous. On the one hand, it might be due to the same OH dangling bond stretch shifted to higher frequencies. Kumi et al.[13] observed red shifts of such OH bands as a consequence of CO_2 or N_2O deposition (see Figures 7 and 14 of ref 13). These would correspond to the blue shift that we detect on warming and therefore on releasing carbon dioxide from the sample. On the other hand, in line with the interpretation provided by Bernstein et al.,[15] a different optical assignment can be put forward. Sharp lines due to two-phonon transitions, like those seen at 87 K, are assigned to two quantum excitations on a single molecule, which would in this case correspond to $\Delta v_1 = 1$, $\Delta v_3 = 1$ and $\Delta v_2 = 2$, $\Delta v_3 = 1$ for $\nu_1 + \nu_3$ and $2\nu_2 + \nu_3$ of CO_2-ext, respectively. On the contrary, broad absorptions of the two-phonon type are attributed to excitations on two different molecules. The broad feature in the 105 K trace could therefore correspond to a $\Delta v_1 = 1$ excitation on one molecule and a $\Delta v_3 = 1$ excitation on another one, both of the CO_2-int type, appearing thus red shifted with respect to those of CO_2-ext. The missing companion, on the low-frequency side of $2\nu_2 + \nu_3$, is probably too weak to be noticed.

Summary and Conclusions

At the low temperature of the present experiments, 87 K, the ν_3 band of CO_2 presents usually a complicated aspect in P-polarized RAIR spectra. A crystalline structure, designated as CO_2-ext, gives rise to a sharper peak at the frequency of ν_{TO} and a broader band between that peak and that of the theoretical ν_{LO}, with somewhat different aspect and variable intensity. An individual peak is visible in this region in some cases, shifting to frequencies larger than ν_{LO}. The broad band between ν_{TO} and ν_{LO} indicates the presence of CO_2 microcrystals in an inhomogeneous surrounding, and the individual peak at $\nu > \nu_{LO}$ is caused by interference effects due to reflections on the Al plate and on the sample, its frequency changing with the thickness of the crystal. This effect is only seen in spectra recorded using P-polarized incident radiation.

On the other hand, after heating at 105 K the spectra become much simplified, with a single band remaining of fairly constant shape, at a frequency slightly lower than ν_{TO}, attributed to CO_2-int. For the sequential crystalline sample, a null trace is left after heating. Further to the evidence presented in ref 14, where transmission spectra were analyzed, the RAIR spectra show that this second CO_2 structure is not forming slabs or regular periodic structures which could involve dipole−dipole interactions among their molecular vibrations. This "interior" CO_2, which remains after heating to the temperature of phase change in water, must therefore be contained inside channels or microcapsules within the amorphous water structure. The small red shift in the observed peak of the CO_2-int with respect to that of the CO_2-ext indicates also a slightly weaker bond between the C and O atoms, possibly because of charge transfer from C−O to O−H bonds in the surrounding water structure. The process of formation of these two different CO_2 structures in sequential deposition experiments seems straightforward, with CO_2-ext remaining mainly in contact with water surfaces and CO_2-int penetrating into the pores of ASW. It is not so obvious for co-deposition, where water and CO_2 molecules reach the Al plate simultaneously.

Spectra in the region of the ν_2 band and in that of the combination bands $\nu_1 + \nu_3$ and $2\nu_2 + \nu_3$ also display effects similar to those observed in the ν_3 region. After heating of the samples, the ν_2 band of CO_2-int is not split into its two components and has an aspect more similar to that of gas-phase CO_2, although at the frequency characteristic of the solid.

The RAIR spectra shown in this investigation provide a good indication of the importance of optical effects in this type of spectroscopic technique, which make it more difficult to interpret than the standard normal incidence transmission setup.

Calculations of a CO_2 crystal made with the SIESTA method produce reasonable results, when using high-level basis sets and tight parameters for the geometry relaxations. Quadrupolar

interactions prove to play an important role in these DFT calculations for CO_2. The usefulness of this methodology even for molecular crystals with weak van der Waals forces is therefore promising.

The distortions produced in the spectral structure of water/carbon dioxide mixtures with respect to their individual spectra constitute a complicated subject. The present research is focused on the spectral bands of CO_2 and in this sense provides a complementary study to the recent work of Öberg et al.,[51] centered on the effects of carbon dioxide on the water bands. There remain several open questions in this field, in spite of the numerous qualified works in the previous literature (see refs 1, 13, and 15 and references therein) and the present contribution. For example, the structure of the so-called CO_2-int and its association with water, is not yet clarified, nor is the assignment of the broad band near $\nu_1 + \nu_3$ remaining after warming at 105 K. Further calculations to those of Signorell, Bauerecker, and co-workers[29−35] would also be needed, especially combining high-level molecular interactions with clusters or crystalline structures. Our results can only be considered as a first step in this direction.

Acknowledgment. This research has been carried out with funding from the Spanish Ministry of Education, Projects FIS2004-00456 and FIS2007-61686. O.G. and R.E. acknowledge financial support from the same Ministry, the "Juan de la Cierva" program and a Sabbatical Grant, respectively. B.M.-Ll. acknowledges a studentship from Comunidad de Madrid and Fondo Social Europeo. We would like to express our gratitude to the Department of Earth Sciences of the University of Cambridge, U.K., for hospitality.

References and Notes

(1) Sandford, S. A.; Allamandola, L. J. *Astrophys. J.* **1990**, *355*, 357.
(2) Bar-Nun, A.; Laufer, D. *Icarus* **2003**, *161*, 157.
(3) Andersson, P. U.; Någård, M. B.; Witt, G.; Petersson, J. B. C. *J. Phys. Chem. A* **2004**, *108*, 4627.
(4) See: Colangeli, L.; Brucato, J. L.; Bar-Nun, A.; Hudson, R. L.; Moore, M. H. *Comets II*; Festou, M. C., Keller, H. U., Weaver, H. A., Eds.; University of Arizona Press: Tucson, 2005; pp 695−717. See also: Meech, K.; Svoren, J. *Comets II*; Festou, M. C., Keller, H. U., Weaver, H. A., Eds.; University of Arizona Press: Tucson, 2005; pp 317−355.
(5) Crovisier, *J. Mol. Phys.* **2006**, *104*, 2737.
(6) Chaban, G. M.; Bernstein, M.; Cruikshank, D. P. *Icarus* **2007**, *187*, 592.
(7) Mousis, O.; Alibert, Y. *Astron. Astrophys.* **2006**, *448*, 771.
(8) Gerakines, P. A.; Bray, J. J.; Davis, A.; Richey, C. R. *Astrophys. J.* **2005**, *620*, 1140.
(9) Boogert, A. C. A.; Ehrenfreund, P. Interstellar Ices. In *Astronomical Society of the Pacific Conference Series 309*; Witt, A. N., Clayton, G. C., Draine, B. T., Eds.; Astronomical Society of the Pacific: San Francisco, CA, 2004; p 547.
(10) Ehrenfreund, P.; Fraser, H. J.; Blum, J.; Cartwright, J. H. E.; García-Ruiz, J. M.; Hadamcik, E.; Levasseur-Regourd, A. C.; Price, S.; Prodi, F.; Sarkissian, A. *Planet. Space Sci.* **2003**, *51*, 473.
(11) Knez, C.; Boogert, A. C. A.; Pontoppidan, K. M.; Kessler-Silacci, J.; van Dishoeck, E. F.; Evans, N. J., II; Augereau, J.-C.; Blake, G. A.; Lahuis, F. *Astrophys. J. Lett.* **2005**, 0511647.
(12) Collings, M. P.; Anderson, M. A.; Cher, R.; Dever, J. W.; Viti, S.; Williams, D. A.; McCoustra, M. R. S. *Mon. Not. R. Astron. Soc.* **2004**, *354*, 1133.
(13) Kumi, G.; Malyk, S.; Hawkins, S.; Reisler, H.; Wittig, C. *J. Phys. Chem. A* **2006**, *110*, 2097.
(14) Gálvez, O.; Ortega, I. K.; Maté, B.; Moreno, M. A.; Martín-Llorente, B.; Herrero, V. J.; Escribano, R.; Gutiérrez, P. J. *Astron. Astrophys.* **2007**, *472*, 691.
(15) Bernstein, M. P.; Cruikshank, D. P.; Sandford, S. A. *Icarus* **2005**, *179*, 527.
(16) Decius, J. C.; Hexter, R. M. *Molecular Vibrations in Crystals*; McGraw-Hill: New York, 1977.
(17) Ovchinnikov, M. A.; Wight, C. A. *J. Chem. Phys.* **1994**, *100*, 972.
(18) Ovchinnikov, M. A.; Wight, C. A. *J. Chem. Phys.* **1993**, *99*, 3374.
(19) Ordejón, P.; Artacho, E.; Soler, J. M. *Phys. Rev. B* **1996**, *53*, 10441.
(20) Soler, J. M.; Artacho, E.; Gale, J. D.; García, A.; Junquera, J.; Ordejón, P.; Sánchez-Portal, D. *J. Phys.: Condens. Matter* **2002**, *14*, 2745.
(21) Simon, A.; Peters, K. *Acta Crystallogr.* **1980**, *B36*, 2750.
(22) Perdew, J. P.; Burke, K.; Ernzerhof, M. *Phys. Rev. Lett.* **1996**, *77*, 3865.
(23) Gygi, F. *Comput. Mater. Sci.* **1998**, *10*, 63.
(24) Junquera, J.; Paz, Ó.; Sánchez-Portal, D.; Artacho, E. *Phys. Rev. B* **2001**, *64*, 235111.
(25) Fernández-Torre, D.; Escribano, R.; Archer, A.; Pruneda, J. M.; Artacho, A. *J. Phys. Chem. A* **2004**, *108*, 10535.
(26) King-Smith, R. D.; Vanderbilt, D. *Phys. Rev. B* **1993**, *47*, 1561.
(27) Fox, D.; Hexter, R. M. *J. Chem. Phys.* **1964**, *41*, 1125.
(28) Kittel, C. *Introduction to Solid State Physics*; Wiley & Sons: New York, 1956.
(29) Kunzmann, M. K.; Signorell, R.; Taraschewski, M.; Bauerecker, S. *Phys. Chem. Chem. Phys.* **2001**, *3*, 3742.
(30) Signorell, R.; Kunzmann, M. K. *Chem. Phys. Lett.* **2003**, *371*, 260.
(31) Bonnamy, A.; Jetzki, M.; Signorell, R. *Chem. Phys. Lett.* **2003**, *382*, 547.
(32) Signorell, R. *J. Chem. Phys.* **2003**, *118*, 2707.
(33) Signorell, R.; Jetzki, M.; Kunzmann, M.; Ueberschaer, R. *J. Phys. Chem. A* **2006**, *110*, 2890.
(34) Bauerecker, S. *Phys. Rev. Lett.* **2005**, *94*, 033404.
(35) Taraschewski, M.; Cammenga, H. K.; Tuckermann, R.; Bauerecker, S. *J. Phys. Chem. A* **2005**, *109*, 3337.
(36) Ehrenfreund, P.; Boogert, A. C. A.; Gerakines, P. A.; Tielens, A. G. G. M.; van Dishoeck, E. F. *Astron. Astrophys.* **1997**, *328*, 649.
(37) Baratta, G. A.; Palumbo, M. E. *J. Opt. Soc. Am. A* **1998**, *15*, 3076.
(38) Maté, B.; Medialdea, A.; Moreno, M. A.; Escribano, R.; Herrero, V. J. *J. Phys. Chem. B* **2003**, *107*, 11098.
(39) McIntyre, J. D. E.; Aspens, D. E. *Surf. Sci.* **1971**, *24*, 417.
(40) Carrasco, E.; Castillo, J. M.; Escribano, R.; Herrero, V. J.; Moreno, M. A.; Rodríguez, J. *Rev. Sci. Instrum.* **2002**, *73*, 3469.
(41) Maté, B.; Ortega, I. K.; Moreno, M. A.; Herrero, V. J.; Escribano, R. *J. Phys. Chem. B* **2006**, *110*, 7396.
(42) Kuchta, B.; Etters, R. D. *Phys. Rev. B* **1998**, *38*, 6265.
(43) Etters, R. D.; Kuchta, B. *J. Chem. Phys.* **1989**, *90*, 4537.
(44) Hirano, T.; Tsuzuki, S.; Tanabe, K.; Tajima, N. *Chem. Lett.* **1995**, *12*, 1073.
(45) Gracia, L.; Marques, M.; Beltran, A.; Pendas, A. M.; Recio, J. M. *J. Phys.: Condens. Matter* **2004**, *16*, S1263.
(46) Dows, D.; Schettino, V. *J. Chem. Phys.* **1973**, *58*, 5009.
(47) Yamada, H.; Person, W. B. *J. Chem. Phys.* **1964**, *41*, 2478.
(48) Bohren, C. F.; Huffman, D. R. *Absorption and Scattering of Light by Small Particles*; Wiley-Interscience: New York, 1998.
(49) Simulations for Mie scattering spectra have been carried out with a program donated by J. J. Sloan.
(50) Mitlin, S.; Leung, K. T. *J. Phys. Chem. B* **2002**, *106*, 6234.
(51) Öberg, K. I.; Fraser, H. J.; Boogert, A. C. A.; Bisschop, S. E.; Fuchs, G. W.; van Dishoeck, E. F.; Linnartz, H. *Astron. Astrophys.* **2007**, *462*, 1187.
(52) Brown, D. E.; George, S. M; Huang, C.; Wong, E. K. I.; Rider, K. B.; Smith, R. S.; Kay, B. D. *J. Phys. Chem.* **1996**, *100*, 4988.
(53) Barrett, C. S.; Meyer, L. *J. Chem. Phys.* **1965**, *43*, 3502.
(54) Meyer, E.; Pletzer, R. *Nature* **1986**, *319*, 298.
(55) Manca, A.; Martin, C.; Roubin, P. *Chem. Phys. Lett.* **2002**, *346*, 224.
(56) Murray, B. J.; Plane, J. M. C. *Phys. Chem. Chem. Phys.* **2003**, *5*, 4129.
(57) Boxe, C. S.; Bodsgard, B. R.; Smythe, W.; Leu, M. T. *Colloid Interface Sci.* **2007**, *309*, 412.
(58) Suëtaka, W. *Surface Infrared and Raman Spectroscopy: Methods and Applications*; Plenum: New York and London, 1955.
(59) Bogan, F.; Schettino, V. *J. Phys. C: Solid State Phys.* **1978**, *11*, 1275.